Bioelectrochemistry 152 (2023) 108432

Contents lists available at ScienceDirect

Bioelectrochemistry

journal homepage: www.journals.elsevier.com/bioelectrochemistry

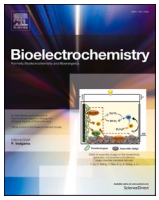

Electro-enzymatic ATP regeneration coupled to biocatalytic phosphorylation reactions

Gabriel García-Molina [a], Paolo Natale [b,c], Ana M. Coito [d], Daniel G. Cava [a], Inés A. C. Pereira [d], Iván López-Montero [b,c,e], Marisela Vélez [a], Marcos Pita [a], Antonio L. De Lacey [a,*]

[a] Instituto de Catálisis y Petroleoquímica, CSIC, c/Marie Curie 2, 28049 Madrid, Spain
[b] Dto. Química Física, Universidad Complutense de Madrid, Avda. Complutense s/n, 28040 Madrid, Spain
[c] Instituto de Investigación Biomédica Hospital Doce de Octubre (imas12), Avda. de Córdoba s/n, 28041 Madrid, Spain
[d] Instituto de Tecnologia Química e Biologica António Xavier, Universidade Nova de Lisboa, 2780-157 Oeiras, Portugal
[e] Instituto Pluridisciplinar. Po. Juan XXIII,1, 28040 Madrid, Spain

ARTICLE INFO

Keywords:
ATP regeneration
ATP-synthase
Hydrogenase
Kinase
Phosphorylation

ABSTRACT

Adenosine-5-triphosphate (ATP) is the main energy vector in biological systems, thus its regeneration is an important issue for the application of many enzymes of interest in biocatalysis and synthetic biology. We have developed an electroenzymatic ATP regeneration system consisting in a gold electrode modified with a floating phospholipid bilayer that allows coupling the catalytic activity of two membrane-bound enzymes: NiFeSe hydrogenase from *Desulfovibrio vulgaris* and F_1F_o-ATP synthase from *Escherichia coli*. Thus, H_2 is used as a fuel for producing ATP. This electro-enzymatic assembly is studied as ATP regeneration system of phosphorylation reactions catalysed by kinases, such as hexokinase and NAD^+-kinase for respectively producing glucose-6-phosphate and $NADP^+$.

1. Introduction

The role of biocatalysis is established in chemical and pharmaceutical industries, manufacturing over 50,000 tonne/year in commodities and high-value chemicals [1]. However, cofactor regeneration is one of the main issues that limits the application of many enzymes in biocatalytic processes and synthetic biology [2–4]. Adenosine-5-triphosphate (ATP) is one of the most important cofactors in nature. It is not only essential as an energy vector for driving up-hill enzymatic reactions, as it is also involved in the synthesis of RNA and DNA, phosphorous-containing biological intermediates and other cofactors, such as flavin adenine dinucleotide (FAD), nicotinamide adenine dinucleotide (NAD^+) and nicotinamide-adenine-dinucleotide phosphate ($NADP^+$) [5]. The use of stoichiometric amounts of enzyme cofactors is inefficient for industrial processes, thus a regeneration system should be included. Most *in vitro* ATP regeneration systems are based in the coupling of a second enzymatic reaction in which ATP is synthesized from ADP and phosphate. The main enzymes used for this purpose are kinases, specially those that use low cost substrates such as polyphosphate, acetyl phosphate and creatine phosphate [4–6]. However, these ATP regeneration systems used in batch require additional steps for the separation of the desired product of the biocatalytic process from the compounds involved in the cofactor recycling. Moreover, kinases are often catalytically reversible enzymes and an equilibrium between ATP synthesis and hydrolysis may be reached.

Alternatively, light-driven ATP regeneration systems have been reported, which are mostly based on the reconstitution of F_1F_o-ATP synthase and bacteriorhodopsin in liposomes [7–9]. Although these systems have the advantage of using sunlight as energy source, the low photon efficiency of bacteriorhodopsin as proton pump greatly limits the rate of ATP synthesis, also the proteoliposomes' stability is low [4,10]. Another interesting alternative is the development of chemically-driven ATP regeneration strategies based on biomimetic systems that focus on compartmentalized and immobilized membrane enzymes. They comprise a semi-permeable biological or biomimetic membrane that allows generating a transmembrane proton gradient in presence of a fuel or light, which drives the ATP synthesis [10–13]. Several of these strategies involve the co-reconstitution of ATP-synthase with a second membrane-bound enzyme that generates the proton gradient, such as cytochrome Qbc [14], cytochrome *c* oxidase [15,16], NADH

* Corresponding author.
E-mail address: alopez@icp.csic.es (A.L. De Lacey).

https://doi.org/10.1016/j.bioelechem.2023.108432
Received 28 July 2022; Received in revised form 29 March 2023; Accepted 30 March 2023
Available online 4 April 2023

dehydrogenase [17] or bo_3 oxidase [18]. F_1F_o-ATP synthase has also been immobilized on an artificial semi-permeable membrane in an electrochemical cell, in which an electrochemical potential gradient was induced to drive ATP synthesis [19]. Electrochemical systems for co-factors regeneration or substrate generation, such as hydrogen peroxide for peroxygenases, are very suitable for biocatalytic processes because they allow *in situ* control in real time [20–22]. Therefore, they are adequate for operating in biocatalytic cascade reactions and in continuous flow-through devices with high atomic and energy efficiency [3,23,24].

In this context, we have previously reported that the combined immobilization of the membrane-bound NiFeSe hydrogenase from *Desulfovibrio vulgaris* with F_1F_o-ATP synthase from *Escherichia coli* allows using the oxidation of H_2 as a fuel for producing ATP. The ATP regeneration system consisted in a gold electrode modified with a floating phospholipid bilayer (PhLB) that allows coupling the catalytic activity of the two membrane-bound enzymes. The deposited biomimetic membrane serves as enzyme support and simultaneously provides a confined aqueous phase close to the electrode [25]. The H_2 oxidation activity of the hydrogenase covalently bound to the electrode surface generates a change of the local pH of 1–2 at the aqueous interface between the electrode and the floating PhLB [26], leading to a proton gradient across the biomimetic membrane that triggers ATP production by the embedded ATP-synthase [25].

In the present work we show the applicability of this electro-enzymatic biomimetic assembly as an ATP regeneration system coupled to phosphorylation reactions catalysed by kinases, such as hexokinase and NAD^+-kinase for respectively producing glucose-6-phosphate and $NADP^+$.

2. Materials and methods

2.1. Chemicals

NaOH 99%, 2-(N-morpholino)ethanesulfonic acid (MES buffer), 4-aminothiophenol 97% (4-APh), adenosine 5′-triphosphate disodium salt hydrate (ATP) BioXtra ≥ 99%, Adenosine 5′-diphosphate sodium salt (ADP) bacterial, ≥95% (ADP), NAD^+ Grade II, free acid, $NADP^+$ disodium salt, magnesium chloride hexahydrate, D-(+)-Glucose ≥ 99.5%, D-Glucose 6-phosphate disodium salt hydrate (G6P), n-dodecyl-β-D-maltoside (DDM), N-(3-dimethylaminopropyl)-N′-ethyl-carbodiimide hydrochloride (EDC), N-hydroxysuccinimide (NHS) 98%, chloroform absolute grade, methanol absolute grade, ethanol absolute grade, H_2NaPO_4 99%, Na_2HPO_4 99%, H_2KPO_4 99% and K_2HPO_4 99% were purchased from Merck. The Bio-Beads SM-2 adsorbents used were from Bio-Rad, and sulfuric acid 96% and hydrogen peroxide 33% were supplied by Panreac. The MicroPolish alumina suspensions were obtained from Buehler. All solutions were prepared with Milli-Q grade water (18.2 MΩ·cm, Millipore).

2.2. Enzymes

F_1F_o-ATP synthase (ATPase) from *E. coli* was purified as described by Gutiérrez-Sanz et al. [25].

For purification of the membrane NiFeSe-hydrogenase (Hase) from *D. vulgaris* Hildenborough was grown anaerobically at 37 °C in standard lactate − sulfate medium supplemented with 10 μM $NiCl_2{\cdot}6H_2O$, 10 μM W and 10 μM $NaSeO_3{\cdot}5H_2O$. Cells were suspended in 20 mM Tris–HCl pH 7.6 with DNase and were disrupted by three passages through a French Press applying 6.9 MPa. The preparation of membrane extract was performed as described in Zacarias et al. [27]. All purification procedures were performed at a pH of 7.6 and at 4 °C in the presence of 0.2% (w/v) SB3–12. The purification was performed aerobically using ion-exchange chromatography columns. The extract with solubilized membrane proteins was loaded on a Q-Sepharose HP column (XK 26/10—GE Healthcare) equilibrated with buffer A (20 mM Tris–HCl pH 7.6, 0.2% (w/v) SB3–12) and a stepwise gradient of NaCl was performed (0–350 mM, with 50 mM steps). The fraction of interest was eluted around 300 mM NaCl and concentrated in an Amicon® ultrafiltration cell with a 30 kDa cut-off membrane, where the ionic strength was also adjusted. SDS-PAGE and activity-stained native gels were performed to evaluate the purity. The fraction from the first chromatographic step was loaded in a second Q-Sepharose HP column (XK 16/10—GE Healthcare) equilibrated with 20 mM Tris–HCl pH 7.6, 0.1% (w/v) n-dodecyl β-D-maltoside (DDM) and a stepwise NaCl gradient was performed as described above to yield pure Hase as judged by SDS-PAGE and activity-stained native gel.

The following enzymes were purchased from Merck: hexokinase from *Saccharomyces cerevisiae* type F-300 lyophilized powder, ≥130 units·mg^{-1} protein (biuret); human NAD^+ kinase, recombinant, expressed in *E. coli*, ≥95% purity (SDS-PAGE); glucose-6-phosphate dehydrogenase (G6P-DH) from *Leuconostoc mesenteroides*, lyophilized powder, ≥550 units·mg^{-1} protein (biuret); glucose-6-phosphate dehydrogenase from baker's yeast (*S. cerevisiae*) type VII, ammonium sulfate suspension, ≥200 units·mg^{-1} protein,

2.3. Preparation of liposomes and proteoliposomes

90 μL of 10 mg·mL^{-1} L-α-phosphatidylcholine (PC) and 9 μL of L-α-phosphatidic acid (PA) from chicken egg (Avanti Polar Lipids) PC in 1:1 (v) of chloroform: methanol were added to 200 μL of the same solution in a Florence Flask, which was inside an ice bath to maintain the stability of the lipids. The solution was dried with a very light N_2 flow, while turning the flask around its own axis to achieve a more homogeneous drying. After this, the flask was left for 40 min under N_2 flow in ice. The dried lipids were re-suspended in 250 μL of 0.1 M sodium phosphate buffer pH 5.5 and stirred during 40 min in a vortex at 500 rpm to let the liposomes be formed. After, the liposomes were passed through a membrane with a pore diameter of 1 μm using an Avanti extruder to obtain a quasi-monodisperse suspension of unilamellar vesicles, and then diluted with 365 μL of 0.1 M sodium phosphate buffer pH 7.6 and 10 μL of 10 mg·mL^{-1} DDM in the same buffer to obtain a final concentration of 1 mg·mL^{-1} liposomes. The suspension was finally stirred for 30 min with a 2 mm micro magnet in a 1.5 mL Eppendorf at 90 rpm.

To obtain the proteoliposomes, ATPase was added to reach a concentration of 11 μg·mL^{-1} and it was let to mix under 90 rpm magnetic stirring during 1 h. Afterwards the suspension was diluted with 0.1 M sodium phosphate buffer pH 5.5 to a final concentration of 0.4 mg·mL^{-1}. The last step was the removal of the DDM detergent from the solution with Bio-Beads®. A small spatula tip of these Bio-Beads® was dropped into the suspension and stirred for 30 min with the micro magnet at 90 rpm. After the first 30 min, the proteoliposomes solution was changed to a new Eppendorf, removing the used Bio-Beads® while adding new Bio-Beads® and stirring again for 30 min at 90 rpm. This process was repeated twice, but the last time the agitation was left overnight. Finally the suspension was transferred to a new Eppendorf without any Bio-Beads® and stored at 5 °C. The proteoliposomes could be used without compromising their performance for approximately one week.

2.4. Preparation of Au/4-APh/Hase/PhBL-ATPase electrodes

Rotating disk electrodes of polycrystalline gold of 0.5 cm diameter (Pine Instruments) were cleaned and modified with a 4-APh self-assembled monolayer (SAM) as reported previously [28]. The electroactive area of the clean bare electrodes measured by cyclic voltammetry (CV) was 0.24 ± 0.03 cm^2 (n = 60 experiments) in sulfuric acid. A drop of 15 μL of 25 μM Hase in 10 mM MES buffer pH 5.5 with 0.1% (m/v) DDM was deposited on top of the electrode modified with the 4-APh SAM and incubated for 20 min. After, it was carefully washed with the same buffer of the enzyme solution. Next, a 17 μL drop of 21 mM EDC in 10 mM MES buffer pH 6.0, 0.1% DDM was placed on top, followed by a

14 μL drop of 11 mM NHS in the same buffer for covalent attachment of the Hase. 30 min later the electrode was carefully washed with the same buffer. Finally, the Au/4-APh/Hase electrode was introduced in a vial containing 1 mL of 0.3 mg·mL^{-1} ATPase proteoliposome solution (5.75 μg of ATP synthase) and approximately 250 mg·mL^{-1} of Bio-Beads®, and it was incubated at 4 °C overnight. Finally the Au/4-APh/Hase/PhBL-ATPase electrode was carefully washed with 0.1 M phosphate buffer pH 7.6. All electrochemical experiments were done with newly-modified electrodes.

2.5. Electrochemical measurements

An Autolab PGSTAT30 potentiostat controlled by Nova 2.1.1 software (Metrohm) equipped with FRA impedance module was used for the electrochemical experiments.

The impedance characterization experiments were performed in a three-electrode cell filled with 6 mL of 2.5 mM potassium ferro/ferricyanide in 0.1 M phosphate buffer pH 7.0. The reference electrode was a BAS Ag/AgCl (3 M NaCl), a platinum wire was used as counter electrode and bare or modified gold disk electrodes were used as working electrodes. A bias potential of + 0.22 V under 10 mV amplitude alternating current was applied, and 30 frequencies logarithmically spared within the range 10 kHz –1 Hz were measured. The experimental impedance spectra were fitted using the Randles electronic equivalent circuit.

The electro-enzymatic ATP regeneration experiments for glucose phosphorylation were done inside a MBraun glove box with $O_2 < 0.1$ ppm with a three-electrode electrochemical cell using platinum wire as counter electrode and a calomel electrode (SCE, Metrohm) as reference electrode, as described previously [29]. The electro-enzymatic ATP regeneration experiments for NAD^+ phosphorylation were done in a smaller three-electrode electrochemical cell with an electrolyte solution volume of 5 mL and temperature-controlled with a Pharmacia Biotech MultiTemp III circulator water bath, also inside the same anaerobic box. The reference electrode was a BAS Ag/AgCl (3 M NaCl) and the counter electrode was a Pt wire. For both glucose and NAD^+ phosphorylation experiments the working electrodes were the modified gold disks connected to a MSR electrode rotator from Pine Instruments. All redox potentials are given relative to the used reference electrode in each case.

2.6. Hexokinase activity measurements

20 mL of a solution with 20 mM D-glucose, 5 mM $MgCl_2$, 0.5–10 mM ATP and 5 U of hexokinase in 0.1 M phosphate buffer pH 7.6 was introduced into a vial and shaken continuously using a roller mixer at 60 rpm at room temperature. 350 μL aliquots were taken every 20–30 min, which were boiled at 100 °C for 5 min to inactivate the hexokinase enzyme before measuring the amount of produced G6P.

The measurements using the Au/4-APh/Hase/PhBL-ATPase electrode as ATP regeneration system were performed inside the glove chamber in an electrochemical cell with 20 mL of 0.1 M potassium phosphate buffer pH 7.6 solution containing 20 mM D-glucose, 5 mM $MgCl_2$ and 0.5 mM ADP, or 0.5 mM ATP in the case of positive controls. The solution was first bubbled for 20 min with N_2 at 25 °C, to ensure that all residual oxygen was removed, and second with H_2 for 20 min to activate the immobilized hydrogenase. After this step, to start the phosphorylation reaction the temperature of the electrochemical cell was raised to 30 °C, 5 U of hexokinase (50 μL) was added to the electrolyte solution, the electrode was rotated at 80 rpm and a chronoamperometry was run at 0.2 V vs. SCE during two hours. Aliquots of 350 μL were taken every 30 min from the electrochemical cell and boiled at 100 °C for 5 min before quantification of the produced G6P.

2.7. NAD^+ kinase activity measurements

5 mL of a 0.1 M potassium phosphate buffer solution pH 7.6 containing 10 mM NAD^+, 5 mM $MgCl_2$ and 1 mM ADP, or 0.5 mM ATP for the positive control experiments, were added to an electrochemical cell inside the glove box with the Au/4-APh/Hase/PhBL-ATPase electrode as ATP regeneration system. The immobilized Hase was activated as described above and the phosphorylation reaction started by addition of 0.25–0.75 U of NAD + kinase (50 μL) and running a chronoamperometry during 2–5 h at 0.23 V vs. Ag/AgCl (3 M Cl^-), under 1 atm H_2, 80 rpm electrode rotation and 30 °C. Aliquots of 150 μL were taken every 30–60 min from the electrochemical cell and immediately analyzed for quantification of $NADP^+$ formed.

2.8. Quantification of G6P formation

2.695 mL of 0.1 M phosphate buffer pH 7.6 containing 6 mM $MgCl_2$ and 3 mM NAD^+ were introduced into a 3 mL quartz cuvette and 300 μL of sample (diluted 10-fold from the phosphorylation reaction aliquots) were added. The cuvette was introduced into a Shimadzu UV-2401PC UV–vis spectrometer with a magnetic stirrer and the temperature controlled at 25 °C by a JP Selecta® Tectron thermostatic bath. The spectrophotometric experiment was started by measuring the absorbance at 340 nm and adding 5 μL (1 unit) of G6P-DH from *L. mesenteroides*. The slope of the NADH absorption increase vs. time was determined from the linear region after the enzyme addition and this value was extrapolated to a calibration standard obtained with known concentrations of G6P.

2.9. Quantification of $NADP^+$ formation

890 μL of 50 mM phosphate buffer pH 7.6 containing 3 mM G6P and 6 mM $MgCl_2$ were introduced to a 1 mL quartz cuvette and 100 μL of the sample (diluted 10-fold from the phosphorylation reaction aliquots) were added. The spectrophotometric assay was run as described for the G6P quantification method, but now 10 μL (2 U) of G6P-DH from *S. cerevesiae* were added for starting the experiment. The slope of the absorption increase vs. time was determined from the linear region after the enzyme addition and this value was extrapolated to a calibration plot previously obtained with known concentrations of $NADP^+$.

2.10. AFM measurements

Tapping mode AFM images were acquired with an Atomic Force Microscope from Agilent Technologies 5500 with the substrate immersed in 0.1 M HEPES buffer solution at pH 7.6. All images were recorded at room temperature employing rectangular gold-coated cantilevers with silicon nitride tips, and a nominal spring constant of 0.28 Nm^{-1} and resonant frequency of 66 kHz in air (APPNANO HYDRA6R). Data acquisition and analysis were performed using PicoView 1.3 (Agilent Technologies) and WSxM 5.0 Develop 8.0 (NanoTech) [30], respectively.

3. Results and discussion

The objective of the work was to study the application of a gold electrode modified with two co-reconstituted membrane enzymes on a floating phospholipid bilayer as an electroenzymatic ATP regeneration system coupled to phosphorylation reactions catalyzed by kinases. The first biocatalytic reaction to be studied was the phosphorylation of glucose to glucose-6-phosphate (G6P) by hexokinase because it is frequently used as a model reaction to test ATP regeneration systems [5,6]. The ATP regeneration system (Schematic 1) is based on the membrane NiFeSe hydrogenase from *D. vulgaris* covalently attached in a oriented way to a gold electrode modified with a SAM of 4-APh to form a monolayer over its surface [25,29], followed by fusion of proteoliposomes of *E. coli* ATP-synthase using the lipid tail of the immobilized hydrogenase as a scaffold for formation of a floating phospholipid bilayer [25].

Impedance spectroscopy and AFM measurements were done to

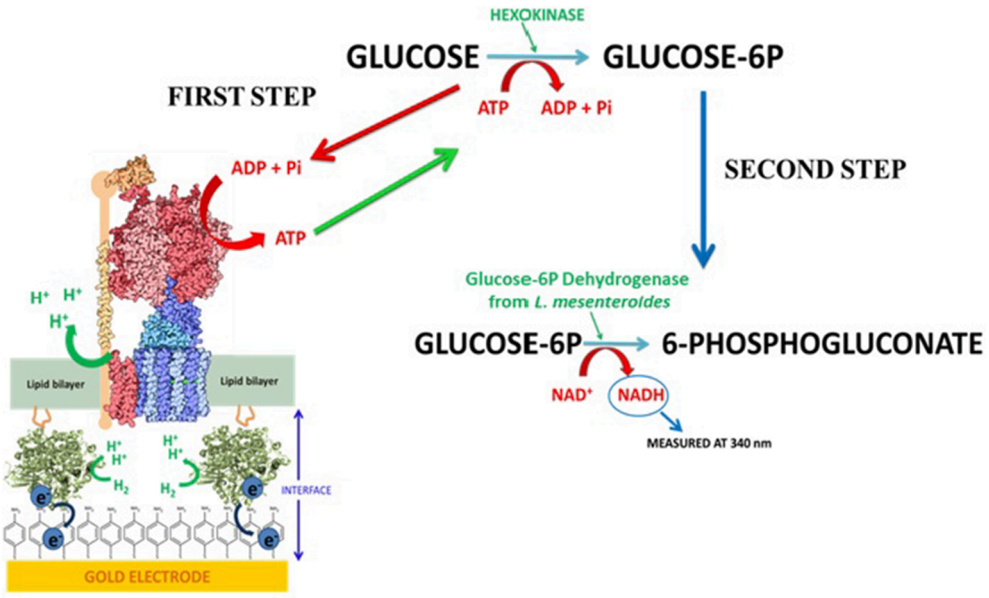

Scheme 1. Phosphorylation of glucose catalyzed by hexokinase coupled to the electroenzymatic ATP regeneration system based on co-immobilized hydrogenase and ATP-synthase on a gold electrode modified with a floating phospholipid bilayer.

characterize the step-by-step construction of the biomimetic membrane enzymes electrode. Fig. 1 shows the Nyquist plots obtained by measuring the electrochemical impedance spectroscopy for each of the different steps of the modified electrode building. A significant decrease of the electron transfer charge resistance on the electrode surface is observed after its modification with the thiol SAM, which is explained by the positively charged 4-APh groups of the monolayer favoring the interaction against the negatively charged redox probe $[Fe(CN)_6]^{3-/4-}$. As expected, the covalent attachment of the Hase monolayer increases the electron transfer resistance, which is significantly increased after the proteoliposomes fusion. This increase of the charge resistance to about 600 Ω can be attributed to formation of a floating phospholipid bilayer [31]. This value is significantly lower than that measured for tethered lipid bilayers, which are much more compact and insulating [32,33]. Some defects are expected in the floating phospholipid bilayer due to the roughness of the gold surface of the electrode, which could make it less insulating. Nevertheless, it is compact enough to allow a net balance of

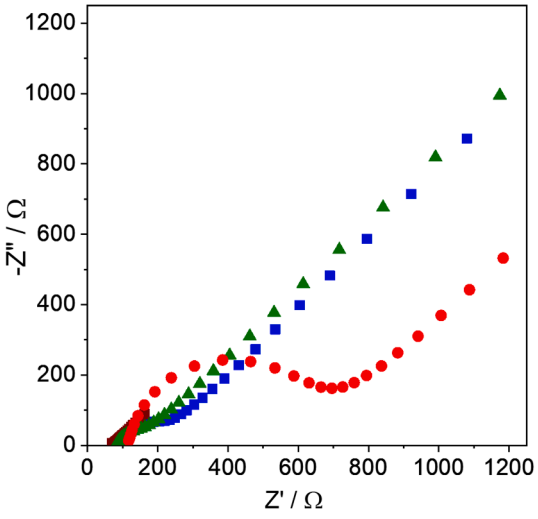

Fig. 1. Faradaic impedance spectra obtained in the presence of 2.5 mM $K_3Fe(CN)_6$ and 2.5 mM $K_4Fe(CN)_6$ for bare Au electrode (blue squares), Au/4-APh electrode (brown squares), Au/4-APh/Hase electrode (green triangles), Au/4-ATP/APh/Hase/PhBL-ATPase electrode (red circles).

protons accumulation in the electrode/phospholipid bilayer interface due to the H_2 oxidation catalytic activity of Hase, as we have previously reported [26].

In a previous work we characterized by AFM the step-by-step modification of Au(1 1 1) plates with the 4-APh monolayer, covalently linked hydrogenase layer and finally after fusion of ATPase proteoliposomes [25]. We now present the AFM study done directly on the gold disk electrodes used for the electrochemical experiments. The images of the gold disk electrode modified with the 4-APh monolayer indicate the presence of regions with low rugosity (1–2 nm) and deep crevices (up to 15 nm) on the surface expected for polycrystalline gold that has been polished with alumina particles of different sizes (Fig. 2 and S1). Although this surface is rougher and has a higher defect density than Au (1 1 1) [25], its topography is significantly modified by the presence of the floating lipid-protein bilayer. The smaller grooves are smoothed and the roughness of the upper layer is increased, being both things compatible with the expected biomimetic construction of Au/4-ATP/APh/Hase/PhBL-ATPase (Fig. 2 and S1). The image after the proteoliposomes fusion shows a film over the electrode surface with protusions, ca. ~ 10 nm, which can be attributed to the large soluble F_1 domain of the ATP-synthase inserted in the phospholipid bilayer [25]. Therefore, the AFM characterization is in agreement with reconstituted ATP-synthase molecules having the adequate orientation with their hydrophilic part facing the external solution. We cannot rule out completely that some ATP synthase molecules may not be in the correct orientation, thus their heads facing the electrode/bilayer interface support, because they would not be observed by AFM. However, the presence of a hydrogenase monolayer underneath the phospholipid bilayer should probably not favor this orientation of the ATP-synthase because of steric impedance. In any case, if some of the ATP-synthase molecules were in the opposite orientation they would be not active in our measurements because ATP/ADP should not permeate across the phospholipid bilayer.

The reaction catalysed by hexokinase consumes 1 ATP molecule per glucose molecule phosphorylated (Schematic 1), and the ADP formed can be recycled to ATP by the Hase/ATPase-modified electrode poised at + 0.2 V vs. SCE in phosphate buffer under H_2 atmosphere [25]. In order to follow the evolution of the phosphorylation reaction, we used a spectrophotometric method for the quantification of G6P. This was done by using a second enzymatic reaction catalysed by G6P-DH from *L. mesenteroides*, in which G6P is converted into 6-phosphogluconate and

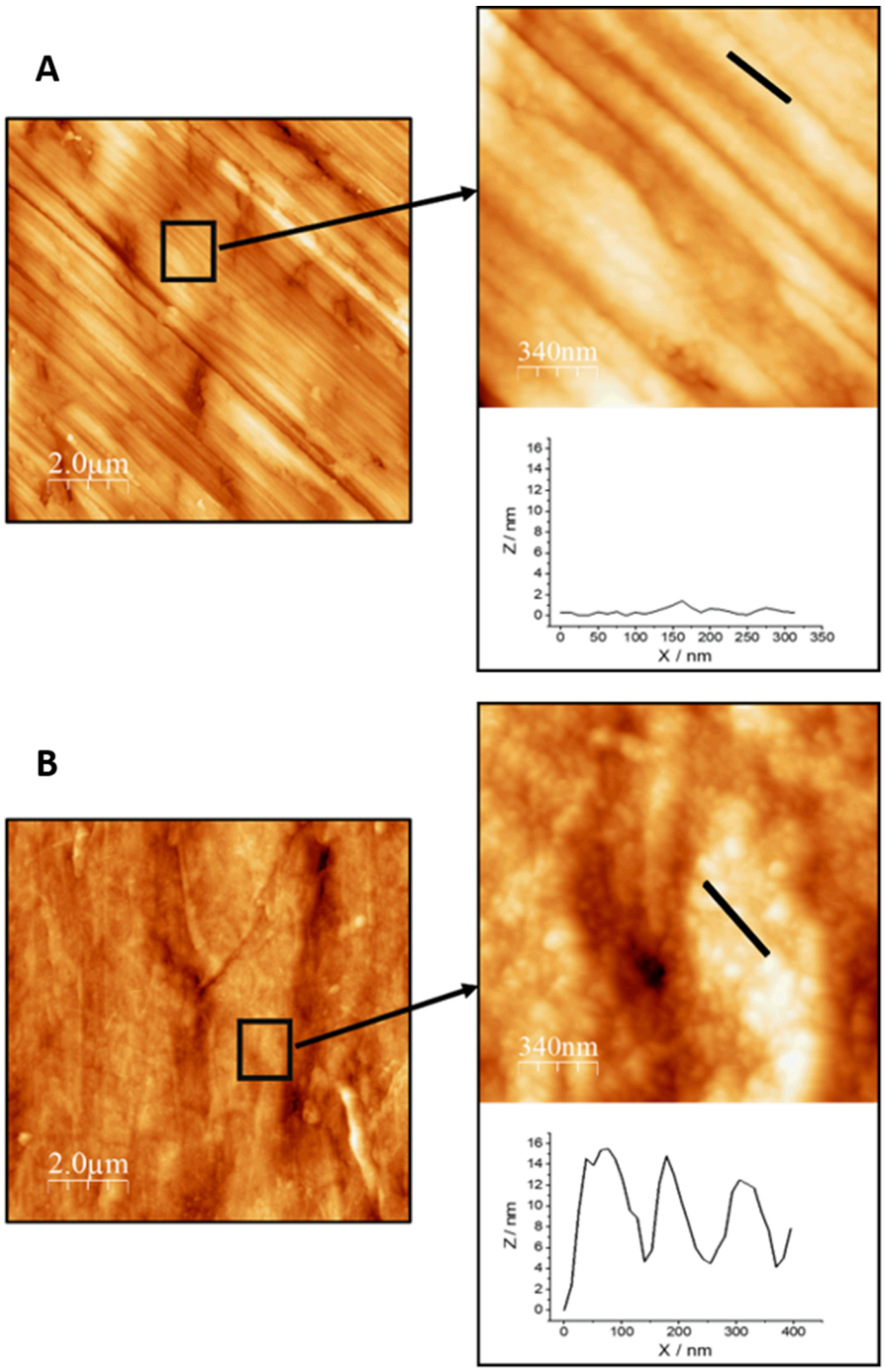

Fig. 2. AFM images of Au disk electrode modified with a 4-APh monolayer (A) and after covalent binding of Hase and fusion of ATPase proteoliposomes (B). The z-axis profiles shown correspond to the black lines in the images.

the NADH cofactor is obtained as by-product (Schematic 1) [6]. A calibration plot was obtained by measuring the rate of NADH production at $\lambda = 340$ nm with known concentrations of G6P. As NAD^+ concentration is in excess, a linear dependence of the NADH formation rate with G6P concentration in the range from 0.0006 to 1.3 mM was measured (Figure S2).

Once the quantification method for G6P was setup, we studied the dependence of the glucose phosphorylation rate catalyzed by hexokinase on the initial ATP concentration. Fig. 3 shows the results obtained with 0.5 and 10 mM ATP, which clearly indicate that at the higher concentration of ATP, G6P was produced at a faster rate. However, we also observe that for both cases the rate of G6P formation decreases considerably after 60 min. With an initial ATP concentration of 10 mM a plateau of G6P concentration around 7 mM is reached, possibly due to hexokinase product inhibition [34]. In the case of lower initial concentration of ATP, almost quantative phosphorylation of glucose was reached after 2 h of reaction. Therefore, all further experiments were performed with an initial concentration of ATP or ADP of 0.5 mM.

The performance of the electroenzymatic ATP regeneration system was tested by adding to the 100 mM phosphate buffer electrolyte solution of the electrochemical cell 5 units of hexokinase, 20 mM glucose and 0.5 mM ADP. After activation of the immobilized hydrogenase

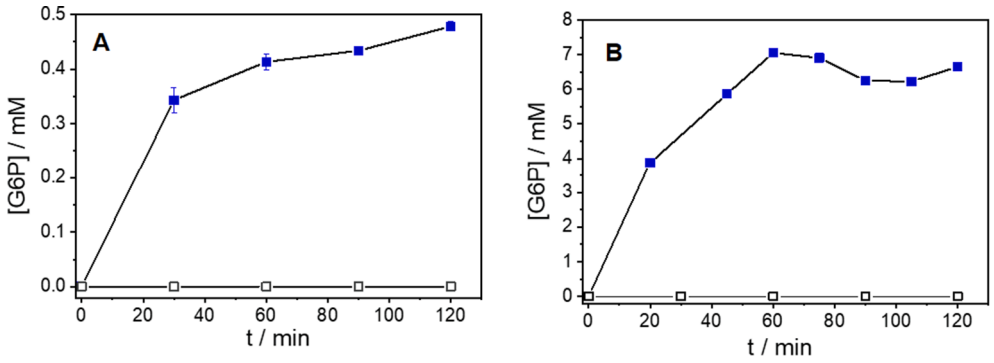

Fig. 3. Rate of glucose-6-phosphate production catalyzed by 5 units of hexokinase with initial ATP concentrations of 0.5 mM (A, blue solid squares) and 10 mM (B, blue solid squares). The initial concentration of glucose was 20 mM. The hollow squares correspond to the control experiments without hexokinase. Error bars correspond to 3 replicate measurements.

under 1 atm of H_2 (Figure S3), a chronoamperometry was run at + 0.2 V vs. SCE with electrode rotation and at 30 °C. This temperature is lower than the optimum temperature for the hydrogenase electrocatalytic activity, but we previously reported that at 40 °C under 1 atm H_2 causes the reductive desorption of the 4-APh SAM [35]. Fig. 4 clearly shows that increasing amounts of G6P are produced during 2 h with the ATP cofactor provided only by the hydrogenase/ATPase electrode. The rate of G6P production measured was 0.027 ± 0.006 μmol × min^{-1}. We do not have a direct measurement of the amount of F_1F_0-ATP-synthase immobilized in the electrode, but we can estimate its coverage from the AFM characterization [11,25]. Taking into account the average electroactive area of the gold disk electrodes and the enzymés molecular weight, we can then estimate around 85 ng of ATP-synthase reconstituted on the electrode with a coverage of roughly 0.7 mol/cm^2 [25]. Therefore, an approximate specific activity of 320 μmol G6P min^{-1} × mg^{-1} (ATPase) is calculated, which is higher than those reported in the literature using light-driven ATP regeneration systems [10] or using acetate kinase in solution as ATP-regeneration system instead of F_1F_0-ATP-synthase [6]. Negative control experiments done in absence of the electrode (Fig. 4) or with one that did not contain reconstituted F_1F_0-ATP-synthase in the phospholipid bilayer (Fig. 5) showed no G6P production. As a positive control experiment, we introduced an initial 0.5 mM ATP in the electrolyte solution instead of ADP. In this case the rate of glucose phosphorylation was much faster, indicating that the electroenzymatic ATP regeneration system limits the rate of the phosphorylation reaction. Nevertheless, after 2 h of reaction the amount of G6P formed exceded the initial ATP concentration, thus indicating cofactor

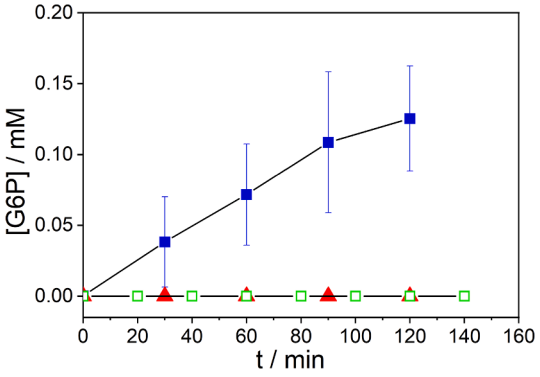

Fig. 4. Rate of glucose-6-phosphate production catalyzed by 5 units of hexokinase with an initial ADP concentration of 0.5 mM in presence of Au/4-Atph/Hase/PhBL-ATPase electrode poised at + 0.2 V vs. SCE, 80 rpm electrode rotation, under 1 atm H_2 and 30 °C (blue solid squares). The initial concentration of glucose was 20 mM. The red triangles and hollow squares correspond to the control experiments without hexokinase or without the enzymatic electrode, respectively. Error bars correspond to 6 replicate measurements.

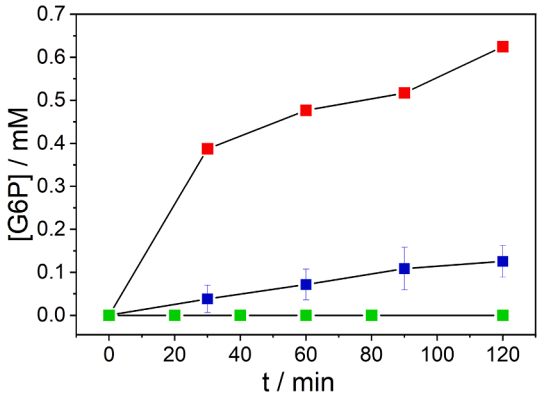

Fig. 5. Rate of glucose-6-phosphate production catalyzed by 5 units of hexokinase in presence of Au/4-Atph/Hase/PhBL-ATPase electrode poised at 0.2 V vs SCE, 80 rpm electrode rotation, under 1 atm H_2 and 30 °C with an initial concentration of 0.5 mM ATP (red squares) or ADP (blue solid squares). The initial concentration of glucose was 20 mM. The green squares correspond to the negative control chronoamperometry performed with a Au/4-Atph/Hase/PhBL electrode (no ATPase) with an initial concentration of 0.5 mM ADP (green squares). Error bars correspond to 6 replicate measurements.

recycling by the coupled reactions (Fig. 5).

The successful coupling of the electro-enzymatic ATP regeneration system to the phosphorylation reaction of glucose led us to couple our electro-enzymatic ATP regeneration system to the commercially interesting synthesis of the cofactor $NADP^+$. The enzyme NAD^+ kinase phosphorylates NAD^+ to $NADP^+$ while consuming 1 ATP molecule per substrate molecule (Schematic 2). To determine the concentration of the produced $NADP^+$ we again used a spectrophotometric assay catalyzed by G6P-DH. In order to specifically discriminate between produced $NADP^+$ and NAD^+ we used G6P-DH of *Saccharomyces cerevesiae* instead of *L. mesenteroides* [36]. By using this $NADP^+$-specific G6P-DH we suppressed the problem of having a very large initial concentration of NAD^+ in the electrolyte solution, which otherwise could not be distinguished from the $NADP^+$ without the use of additional chromatographic methods as HPLC to separate both cofactors [37]. We first performed the calibration plot with known concentrations of $NADP^+$ and in excess of G6P. A linear dependence of the NADPH rate formation with the initial of concentration of $NADP^+$ was measured in the 0.6–10 μM range (Figure S4).

Fig. 6 shows the results obtained for the phosphorylation of NAD^+ catalyzed by NAD^+ kinase coupled to the electro-enzymatic ATP regeneration system poised at 0.23 V vs. Ag/AgCl (3 M Cl^-) under 1 atm H_2. Again, the ATP-regeneration system was able to feed the biocatalytic reaction with ATP, measuring a rate of $NADP^+$ production of 0.6 nmol ×

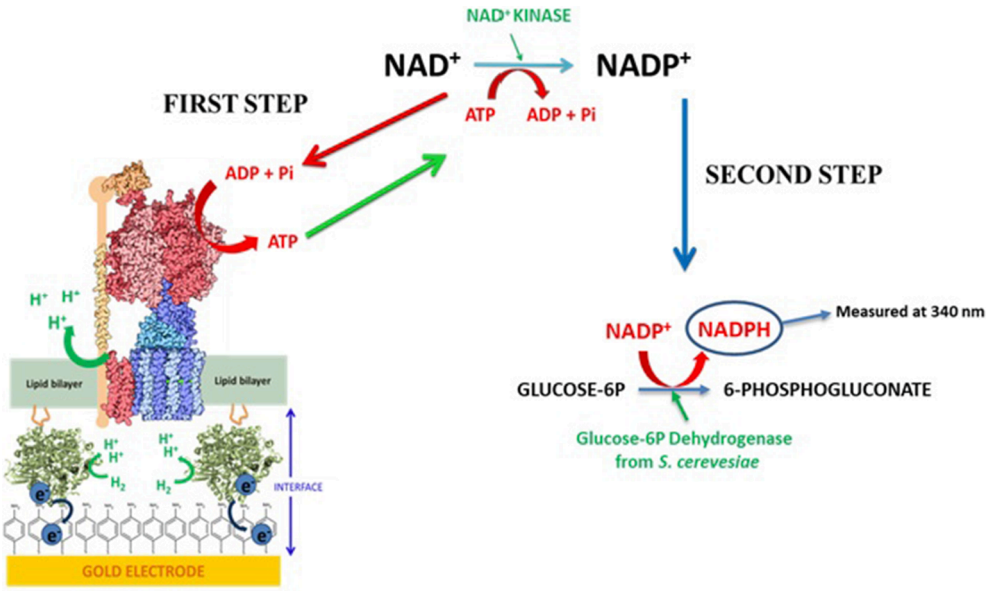

Scheme 2. Phosphorylation of NAD^+ catalyzed by NAD^+-kinase coupled to the electroenzymatic ATP regeneration system based on co-immobilized hydrogenase and ATP-synthase on a gold electrode modified with a floating phospholipid bilayer.

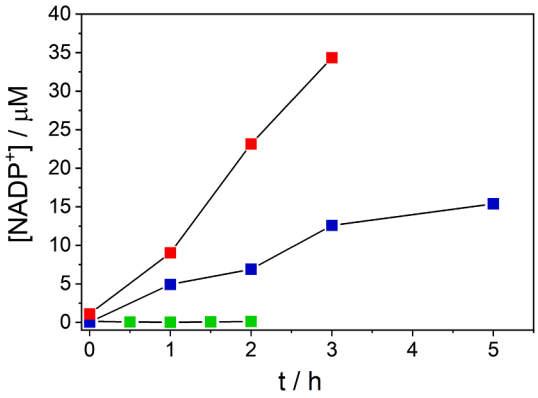

Fig. 6. Rate of $NADP^+$ production catalyzed by NAD^+ kinase in presence of Au/4-Atph/Hase/PhBL-ATPase electrode poised at + 0.23 V vs. Ag/AgCl (3 M Cl^-), under 1 atm H_2, 80 rpm of electrode rotation with an initial concentration of 0.5 mM ATP (red squares, 0.25 enzyme units) or 1 mM ADP (blue squares, 0.75 enzyme units). The initial concentration of NAD^+ was 10 mM. The green squares correspond to the control experiment in absence of NAD^+ kinase (green squares).

min^{-1}. The estimated specific activity is around 5 μmol $NADP^+$ $min^{-1} \cdot mg^{-1}$ (ATPase). The rate of $NADP^+$ production was faster in the positive control with an initial 0.5 mM ATP concentration, indicating again that ATP regeneration limits the overall rate. The electroenzymatic ATP regeneration system was at least operational for 5 h, although the rate of $NADP^+$ production did show some decrease after 3 h. The negative control without the ATP-regeneration system, and with only ADP in the electrolyte, gave negligible values for $NADP^+$ quantification that did not change with time, confirming the very low interference of NAD^+ in the detection assay.

4. Conclusions

We show in this work that the gold electrodes modified with Hase and ATPase co-immobilised with a floating phospholipid bilayer are functional as an ATP-regeneration system for biocatalytic phosphorylations. The rates of G6P and $NADP^+$ production measured were 27 and 0.6 nmol × min^{-1} respectively, using ATP provided only by the electroenzymatic regeneration system. The estimated specific activities of the reconstituted ATPase for the studied phosphorylation reactions are higher than those reported in the literature using other light or chemically driven ATP regeneration systems (Table S1). The use of H_2 as fuel for the ATP-regeneration system and the electrochemical control for driving the process make this electro-enzymatic system suitable for batch processes without requiring additional separation steps of products. However, for practical applications the operational stability of the system at long reaction times (5–24 h) and the re-usability of the electrodes should be tested. Furthermore, to overcome ATP regeneration rate-limiting the biocatalytic reaction, the reactor design should be improved to increase the ratio between the electrode area and the reaction volume. Indeed, these Hase/ATPase-modified electrodes could be applied in flow-through sytems for biocatalytic cascade reactions with *in situ* control of the ATP regeneration in real time.

Declaration of Competing Interest

The authors declare that they have no known competing financial interests or personal relationships that could have appeared to influence the work reported in this paper.

Data availability

Data will be made available on request.

Acknowledgements

A.L.D, M.P. and M.V. thank grants RTI2018-095090-B-I00 and PID2021-1241160B-I00 funded by MCIN/AEI/ 10.13039/501100011033 and by the European Union, and 2021AEP014 funded by CSIC. G.G.M. thanks grant BES-2016-078815 funded by MCIN/AEI/10.13039/501100011033 and by the European Union. I.L.-M. and M.V. acknowledge financial support through grant S2018/BAA-4403 SINOXPHOS-CM (EU-FEDER). I.A.C.P. and A.M.C. thank support from the Fundação para a Ciência e Tecnologia through fellowship SFRH/BD/146475/2019 and MOSTMICRO-ITQB R&D Unit (UIDB/04612/2020, UIDP/04612/2020) and LS4FUTURE Associated Laboratory (LA/P/0087/2020).

Appendix A. Supplementary material

Supplementary data to this article can be found online at https://doi.org/10.1016/j.bioelechem.2023.108432.

References

[1] A.J.J. Straathof, Ttransformation of biomass into commodity chemicals using enzymes or cells, Chem. Rev. 114 (2014) 1871–1908.
[2] S. Velasco-Lozano, A.I. Benítez-Mateos, F. López-Gallego, Co-immobilized phosphorylated cofactors and enzymes as self-sufficient heterogeneous biocatalysts for chemical processes, Angew. Chem. Int. Ed. 56 (2017) 771–775.
[3] B.O. Burek, A.W.H. Dawood, F. Hollmann, A. Liese, D. Holtmann, Process intensification as game changer in enzyme catalysis, Front. Catal. 2 (2022), 858706.
[4] Y.H.P. Zhang, S. Myung, C. You, Z. Zhu, J.A. Rollin, Toward low-cost biomanufacturing through in vitro synthetic biology: bottom-up design, J. Mater. Chem. 21 (2011) 18877–18886.
[5] J.N. Andexer, M. Richter, Emerging enzymes for ATP regeneration in biocatalytic processes, ChemBioChem 16 (2015) 380–386.
[6] B. Yan, Q. Ding, L. Ou, Z. Zou, Production of glucose-6-phosphate by glucokinase coupled with an ATP regeneration system, World J. Microbiol. Botechnol. 30 (2014) 1123–1128.
[7] T.J.M. Luo, R. Soong, E. Lan, B. Dunn, C. Montemagno, Photo-induced proton gradients and ATP biosynthesis produced by vesicles encapsulated in a silica matrix, Nat. Mater. 4 (2005) 220–224.
[8] D. Wendell, J. Todd, C. Montemagno, Artificial photosynthesis in Ranaspumin-2 based foam, Nano Lett. 10 (2010) 3231–3236.
[9] K.A. Lee, K.H. Jung, ATP regeneration system using *E. coli* ATP synthase and *Gloeobacter* rhodopsin and its stability, J. Nanosci. Nanotechnol. 11 (2011) 4261–4264.
[10] L. Otrin, C. Kleineberg, L. Caire da Silva, K. Landfester, I. Ivanov, M. Whang, C. Bednarz, K. Sundmacher, T. Vidakovic-Koch, Artificial organelles for energy regeneration, Adv. Biosys. 3 (2019) 1800323.
[11] Y. Xu, J. Fei, G. Li, T. Yuan, J. Li, Compartmentalized assembly of motor protein reconstituted on protocell membrane toward highly efficient photophosphorylation, ACS Nano 11 (2017) 10175–10183.
[12] V.G. Almendro-Vedia, P. Natale, M. Mell, S. Bonneau, F. Monroy, F. Joubert, I. Lopez-Montero, Non-equilibrium fluctuations of lipid membranes by the rotating motor protein F_1F_o-ATP synthase, Proceed. Natl. Acad. Sci. USA 114 (2017) 11291–11296.
[13] G. Li, J. Fei, Y. Xu, B. Sun, J. Li, Tuning thiol-based self-assembled monolayer chemistry on a gold surface towards the synthesis of biochemical fuel, Angew. Chem. Int. Ed. 58 (2019) 1110–1114.
[14] B.E. Krenn, F. Koppenaal, H.S. Vsn Walraven, K. Krab, R. Kraayenhof, Co-reconstitution of the H+-ATP synthase and cytochrome b-563/c-554 complex from a thermophilic cyanobacterium. High ATP yield and mutual effects on the enzymatic activities, Biochim. Biophys. Acta-Bioenerg. (1993, 1140,) 271–281.
[15] C. von Ballmoos, O. Biner, T. Nilsson, P. Brzezinski, Mimicking respiratory phosphorylation using purified enzymes, Biochim. Biophys. Acta 2016 (1857) 321–331.
[16] T. Nilsson, C.R. Lundin, G. Nordlund, P. Ädelroth, C. von Ballmoos, P. Brzezinski, Lipid mediated protein-protein interactions modulated respiration-driven ATP-synthesis, Sci. Rep. 6 (2016) 24113.
[17] A.C. Gemperli, P. Dimroth, J. Steuber, Sodium ion cycling mediates energy coupling between complex I and ATP synthase, Proceed. Natl. Acad. Sci. USA 100 (2003) 839–844.
[18] L. Otrin, N. Marusic, C. Bednarz, T. Vidakovic-Koch, I. Lieberwirth, K. Landfester, K. Sundmacher, Toward artificial mitochondrion: mimicking oxidative phosphorylation in polymer and hybrid membranes, Nano Lett. 17 (2017) 6816–6821.
[19] S. Bhattacharya, M. Schiavone, A. Nayak, S.K. Bhattacharya, Uniformly oriented bacterial F_0F_1-ATPase immobilized on a semi-permeable membrane: a step towards biotechnological energy transduction, Biotechnol. Appl. Biochem. 39 (2004) 293–301.
[20] D. Holtmann, T. Krieg, L. Getrey, J. Schrader, Electroenzymatic process to overcome enzyme instabilities, Catal. Commun 51 (2014) 82–85.
[21] B. Siritanaratkul, C.F. Megarity, T.G. Roberts, T.O.M. Samuels, M. Winkler, J. H. Warner, T. Happe, F.A. Armstrong, Transfer of photosynthetic $NADP^+$/NADPH recycling activity to a porous metal oxide for highly specific, electrochemically-driven organic synthesis, Chem. Sci. 8 (2017) 4579–4586.
[22] A. Al-Shameri, M.C. Petrich, K.J. Puring, U.P. Apfel, B.M. Nestl, L. Lauterbach, Angew. Chem. Int. Ed. 59 (2020) 10929–10933.
[23] R.A. Rincón, C. Lau, K.E. García, P. Atanassov, Flow-through 3D biofuel cell anode for NAD^+-dependent enzymes, Electrochim. Acta 56 (2011) 2503–2509.
[24] H. du Toit, R. Rashidi, D.W. Ferdani, M.B. Delgado-Charro, C.M. Sagan, M. Di Lorenzo, Generating power from transdermal extracts using a multi-electrode miniature enzymatic fuel cell, Biosens. Bioelectron. 78 (2016) 411–417.
[25] O. Gutiérrez-Sanz, P. Natale, I. Márquez, M.C. Marques, S. Zacarías, M. Pita, I.A. C. Pereira, I. López-Montero, A.L. De Lacey, M. Vélez, H_2 fueled ATP synthesis: mimicking an electrode-assisted cellular respiration, Angew. Chem. Int. Ed. 55 (2016) 6216–6220.
[26] O. Gutiérrez-Sanz, C. Tapia, M.C. Marques, S. Zacarías, M. Vélez, I.A.C. Pereira, A. L. De Lacey, Induction of a proton gradient across a gold-supported biomimetic membrane by electroenzymatic $_H$2 oxidation, Angew. Chem. Int. Ed. 54 (2015) 2684–2687.
[27] S. Zacarias, M. Vélez, M. Pita, A.L. De Lacey, P.M. Matias, I.A.C. Pereira, Characterization of the [NiFeSe] Hydrogenase from *Desulfovibrio vulgaris* Hildenborough, Meth. Enzymol. 613 (2018) 169–201.
[28] G. García-Molina, P. Natale, L. Valenzuela, J. Alvarez-Malmagro, C. Gutiérrez-Sánchez, A. Iglesias-Juez, I. López-Montero, M. Vélez, M. Pita, A.L. De Lacey, Potentiometric detection of ATP based on the transmembrane proton gradient generated by ATPase reconstituted on a gold electrode, Bioelectrochemistry 133 (2020), 107490.
[29] C. Gutiérrez-Sánchez, D. Olea, M. Marques, V.M. Fernández, I.A.C. Pereira, M. Vélez, A.L. De Lacey, Oriented immobilization of a membrane-bound hydrogenase onto an electrode for direct electron transfer, Langmuir 27 (2011) 6449–6457.
[30] I. Horcas, R. Fernandez, J.M. Gomez-Rodriguez, J. Colchero, J. Gomez-Herrero, A. M. Baro, WSXM: A software for scanning probe microscopy and a tool for nanotechnology, Rev. Sci. Instrum. 78 (2007), 013705.
[31] O. Gutiérrez-Sanz, D. Olea, M. Pita, A.P. Batista, A. Alonso, M.M. Pereira, M. Vélez, A.L. De Lacey, Reconstitution of respiratory complex I on a biomimetic membrane supported on gold electrodes, Langmuir 30 (2014) 9007–9015.
[32] L.J.C. Jeuken, R.J. Bushby, S.D. Evans, S. D, Proton transport into a tethered bilayer lipid membrane, Electrochem. Commun. 9 (2007), 610–614.
[33] C. Martensson, V. Agmo Hernandez, Ubiquinone-10 in gold-immobilized lipid membrane structures acts as a sensor for acetylcholine and other tetraalkylammonium cations, Bioelectrochemistry 88 (2012) 171–180.
[34] X. Liu, C.S. Kim, F.T. Kurbanov, R.B. Honzatko, H.J. Fromm, Dual mechanisms for glucose 6-phosphate inhibition of human brain hexokinase, J. Biol. Chem. 274 (1999) 31155–31159.
[35] O. Rüdiger, C. Gutiérrez-Sánchez, D. Olea, I.A.C. Pereira, M. Vélez, V. M. Fernández, A.L. De Lacey, Enzymatic anodes for hydrogen fuel cells based on covalent attachment of Ni-Fe hydrogenases and direct electron transfer to SAM-modified gold electrodes, Electroanalysis 22 (2010) 776–783.
[36] M. Klingenberg, NAD(P), NAD(P)H: End-point UV-methods, Methods of Enzymatic Analysis (1974) 251–271.
[37] Y. Aso, S. Gotoh, N. Yamasaki, A HPLC method for simultaneous analysis of NAD (P)$^+$ and NAD(P)H: Its application to the study of spinach ferredoxin: $NADP^+$ reductase-catalyzed transhydrogenation, Agric. Biol. Chem. 53 (1989) (1989) 1635–1639.